Theoretical and experimental study of slow-scale Hopf limit-cycles in laser-based wideband optoelectronic oscillators

Geraud R. Goune Chengui,[1] Alain F. Talla,[1] Jimmi H. Talla Mbé,[1] Aurélien Coillet,[2,3] Khaldoun Saleh,[2] Laurent Larger,[2] Paul Woafo,[1] and Yanne K. Chembo[2,*]

[1]*Laboratory of Modelling and Simulation in Engineering, Biomimetics and Prototypes, Department of Physics, Faculty of Science, P. O. Box 812, Yaoundé, Cameroon*
[2]*FEMTO-ST Institute (CNRS UMR6174), Optics Department, 16 Route de Gray, 25030 Besançon Cedex, France*
[3]*Currently at NIST, Boulder, Colorado 80305, USA*
Corresponding author: yanne.chembo@femto-st.fr

Optoelectronic oscillators are the subject of extensive research because of the wide variety of associated applications, which include chaos cryptography, ultrastable microwave generation, and neuromorphic computing. The wideband optoelectronic oscillator presents a particular feature allowing for two dynamical time scales to be superimposed, namely, a slow one and a fast one. In this paper, we fully characterize the onset of the slow-scale oscillation in the wideband optoelectronic oscillator. We investigate the dynamics associated to the first Hopf bifurcation and calculate analytically both the amplitude and period of the induced limit-cycle. In particular, we show how the dynamics of the zero-delay case can be used to provide insight into the infinite-dimensional dynamics of the delayed system. Our theoretical results are in very good agreement with the experimental measurements.   © 2014 Optical Society of America

OCIS codes: (120.3940) Metrology; (190.3100) Instabilities and chaos; (350.4010) Microwaves.
http://dx.doi.org/10.1364/JOSAB.31.002310

1. INTRODUCTION

Dynamical systems with delay are abundant in nature, and they have been the object of many investigations in science and technology (see, for example, [1,2] and references therein). A delay differential equation (DDE) with a single constant delay can be represented under the general form

$$\frac{d\mathbf{x}}{dt} = \mathbf{F}[t, \mathbf{x}(t), \mathbf{x}(t - T_D)], \qquad (1)$$

where $\mathbf{x}$ is a N-dimensional variable, $\mathbf{F}$ a N-dimensional algebraic function (generally nonlinear), t is the time, and T_D is the delay. Such delayed systems have been thoroughly studied in optics and photonics, where the time scales can span over several orders of magnitude and thereby require taking into account delay propagation times (see, for example, review articles [3,4]). In particular, delay dynamical systems emerged as a very fertile formalism for the study of narrowband [5–7] and wideband [8–17] optoelectronic oscillators (OEO), which are generally investigated using the paradigm of Ikeda equations [18–20].

However, compared to the original studies on the Ikeda paradigm, its optoelectronic experimental version has introduced two novel and essential dynamical features: (i) the experimentally intrinsic band limited feedback required the introduction of a slow (integral) time scale, and (ii) the previous feature forces the reconsideration of the positive feedback situation as a source of novel dynamical phenomena (the well-known period doubling route to chaos extensively studied with the Ikeda paradigm is indeed concerned with the negative feedback only).

In such a case of wideband OEO, it had been shown that they can be synthetically modeled using an integrodifferential delay equation (iDDE), which is characterized by three time scales: a fast time scale τ related to the high cutoff frequency (linked to the derivative term), a slow time scale θ related to the low cutoff frequency (linked to the integral term), and a third time scale defined by the delay generally much slower than τ (large-delay case). The richness of the observed dynamical solutions appears as a consequence of the interplay between these three time scales, in which the importance is generally ruled by the strength of the nonlinearity in the dynamics (where strength is typically controlled by the gain of the nonlinear function) $\mathbf{F}$.

For weak nonlinearities, delay dynamical systems with an integral term and positive feedback exhibits stable low-frequency periodic oscillations that do not exist in the original Ikeda paradigm. Faster oscillations also appear with positive feedback, even though for higher nonlinear feedback. As the gain is increased from zero, a large variety of motions can indeed be observed whether experimentally or numerically, from fixed points through limit-cycles and torii up to fully developed chaos. In this work, we will focus on the dynamical characterization of the slow limit-cycle emerging from the first Hopf bifurcation, for the wideband configuration of the OEO. Understanding this phenomenology is particularly important in applications were these slow-scale oscillations have to be either avoided or enhanced. In particular, we will focus on the

variation of the amplitude and frequency (or period) evolution as the gain parameter is slightly increased from the Hopf threshold. Our methodology will rely on first studying the zero-delay (two-dimensional) system, and thereby gain insight into the more complex case of the (infinite-dimensional) delayed system.

The outline of the paper is the following. The model of the wideband OEO is briefly presented in Section 2, and we study the Hopf bifurcation in Section 3. In Section 4, we present our OEO experimental setup and discuss the results obtained. Section 5 focuses on the evolution of the oscillation period depending on the various tunable parameters (laser power and bias voltage) in the absence of delay. The case with delay is discussed in Section 6, and the last section concludes the article.

2. MODEL

A schematic view of the OEO configuration analyzed in this paper is shown in Fig. 1. The laser diode (LD) sends a continuous wave (CW) light into an integrated electro-optic Mach–Zehnder modulator (MZM) of half-wave voltages $V_{\pi_{\mathrm{DC}}}$ (DC input) and $V_{\pi_{\mathrm{RF}}}$ (RF input). The nonlinearly modulated optical intensity at the output of the MZM is then sent to an optical fiber which is mainly responsible for the time delay T_D. Subsequently, the light at the end of the optical fiber is detected by a broadband amplified photodiode (PD). This photodiode converts and filters the optical signal into the electrical one. The resulting electrical signal is amplified with gain G by a radio frequency (RF) amplifier and used to drive the MZM [RF voltage $V(t)$]. In the first approximation, the electronic bandwidth of the feedback loop is supposed to result from two cascaded linear first-order low-pass and high-pass filters, with low and high cutoff frequencies f_L and f_H, respectively. The equation describing the dynamics of this OEO can be modeled by the following iDDE [8,10]:

$$x + \tau \frac{dx}{dt} + \frac{1}{\theta} \int_{t_0}^{t} x(s)\mathrm{d}s = \beta \cos^2[x(t - T_D) + \phi], \qquad (2)$$

where $\tau = 1/2\pi f_H$, $\theta = 1/2\pi f_L$, $\phi = \pi V_B/2V_{\pi_{\mathrm{DC}}}$, with V_B being the bias voltage applied to the DC electrode of the MZM. The dimensionless variable of the system $x(t) = \pi V(t)/2V_\pi$ is the normalized voltage applied to the MZM. The main control parameter is the feedback gain $\beta = \pi\kappa SGP/2V_\pi$ which depends on the overall attenuation of the feedback loop κ, the responsivity of the photodiode S, the RF amplifier gain G, and the optical power emitted by the laser P. For numerical simulations, the following parameter values derived from the experimental setup will be considered: $\tau = 1.6$ ns
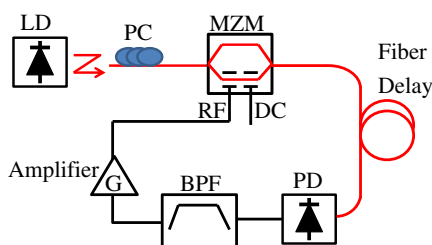

Fig. 1. Experimental setup: LD, laser diode; MZM, Mach–Zehnder modulator; PD, photodiode; PC, polarization controller; BPF, band-pass filter.

($f_H = 100$ MHz), $T_D = 10$ μs (2 km of fiber), and $\theta = 160$ μs ($f_L = 1$ kHz) for the three characteristic time scales (thus spanning over 5 orders of magnitude), and unless otherwise stated, the value of ϕ will be set to $-\pi/4$.

3. HOPF BIFURCATION AND AMPLITUDE OF THE LIMIT-CYCLE

The model presented in the previous section only has a single fixed point, which is the trivial equilibrium $x_{\mathrm{tr}} = 0$. The stability analysis of this fixed point has already been performed in [10], in the configuration where $\tau \ll T_D \ll \theta$ which is also the one we consider in this paper. It was then found that $\gamma = \beta \sin 2\phi$ is a more meaningful bifurcation parameter, since it contains through the factor $\sin 2\phi$ the slope of the nonlinear transfer function at the fixed point, which can be positive or negative depending on ϕ. On one hand, it is also shown that when γ is increased from 0 to $+\infty$, the first bifurcation value is $\gamma_1 \simeq 1$ and corresponds to a Hopf bifurcation which leads to oscillations of frequency $\Omega_1 = \pi/T_D$ (or period $2T_D$). On the other hand, when γ is increased in on the negative side (toward $-\infty$), the first bifurcation value is

$$\gamma_0 = -1 - \frac{1}{2}\frac{T_D}{\theta}, \qquad (3)$$

leading to a Hopf bifurcation of frequency

$$\Omega_0 = \frac{1}{\sqrt{\theta T_D}}. \qquad (4)$$

This latter Hopf bifurcation frequency is indeed very low, and accordingly, reveals the interplay between the slow time scale and the time delay. It was later shown in [10] that as the gain is increased, fast-scale hyperchaotic oscillations appear on top of this slow-scale limit-cycle, leading then to the emergence of chaotic breathers.

In this section, we aim to analytically calculate the amplitude of this limit-cycle in the small amplitude approximation, as verified when considering gain values close to the Hopf bifurcation point. We first consider that the limit-cycle has a stationary sinusoidal solution with constant amplitude A and phase ψ (which can be considered as the reference phase and arbitrarily set to zero, if needed). This solution can be formally written as

$$x(t) = A \cos[\Omega_0 t + \psi] = \frac{1}{2}\mathcal{A}e^{i\Omega_0 t} + \mathrm{c.c.}, \qquad (5)$$

where c.c. stands for the complex conjugate of the preceding term, $\mathcal{A} = Ae^{i\psi}$ is the complex-valued envelope of the slow-scale oscillation, while Ω_0 is its frequency as defined in Eq. (4).

Further analytics can be developed with the Jacobi–Anger expansion

$$e^{iz \cos \alpha} = \sum_{n=-\infty}^{+\infty} i^n J_n(z)e^{in\alpha}, \qquad (6)$$

where J_n is the nth order Bessel function of the first kind, and the nonlinear $\cos^2$ term can be expanded in harmonics of Ω_0 following:

$$\cos^2[x(t - T_D) + \phi] = \mathcal{C}_0 + \sum_{n=1}^{+\infty}\left\{\frac{1}{2}\mathcal{C}_n e^{in\Omega_0 t} + \text{c.c.}\right\}, \quad (7)$$

where

$$\mathcal{C}_0 = \frac{1}{2} + \frac{1}{2}J_0(2A)\cos 2\phi,$$

$$\mathcal{C}_n = \frac{1}{2}J_n(2A)i^n e^{in(\psi - \sigma)}\{e^{2i\phi} + (-1)^n e^{-2i\phi}\}, \qquad n \neq 0. \quad (8)$$

The parameter $\sigma = \Omega_0 T_D$ is the phase shift of the signal after one round trip in the delayed oscillator loop. Then, after inserting Eqs. (5) and (7) into the original Eq. (2), we obtain the following relationship:

$$\left[1 + i\Omega_0\tau + \frac{1}{i\Omega_0\theta}\right]\mathcal{A} = \beta\mathcal{C}_1, \quad (9)$$

after equating oscillating terms of the same fundamental tone frequency Ω_0. In the particular wideband OEO configuration considered here ($\tau \ll T_D \ll \theta$), the term $1/\Omega_0\theta = \Omega_0 T_D = \sigma$ is small compared to 1, but the other term $\Omega_0\tau$ is even smaller, so that it can be neglected. We are therefore left with the equation

$$[1 - i\sigma]\mathcal{A} = -\beta \sin 2\phi J_1(2A)e^{i\psi}e^{-i\sigma}, \quad (10)$$

and in the limit $\sigma \ll \pi$ which is typical for wideband OEOs, we have

$$\frac{e^{-i\sigma}}{1 - i\sigma} \simeq 1 - \frac{\sigma^2}{2} = 1 - \frac{1}{2}\frac{T_D}{\theta}, \quad (11)$$

up to the second order in σ. This truncated Taylor expansion helps us to find the following nonlinear transcendental equation for the real-valued amplitude:

$$J_{c1}(2A) = -\frac{1}{2\gamma\left[1 - \frac{1}{2}\frac{T_D}{\theta}\right]}, \quad (12)$$

where J_{c1} is the Bessel-cardinal function defined by $J_{c1}(x) = J_1(x)/x$.

The Bessel-cardinal function qualitatively looks like the well-known sine-cardinal function, except its maximum is $J_{c1}(0) = 1/2$ instead of 1. The bifurcation parameter threshold is therefore achieved for

$$\frac{1}{2} = -\frac{1}{2\gamma_0\left[1 - \frac{1}{2}\frac{T_D}{\theta}\right]}, \quad (13)$$

yielding the critical value $\gamma_0 = -1 - T_D/2\theta$ that was obtained in [10]. Notice that from Eq. (12), the following explicit relationship can be derived:

$$A = \sqrt{3}\left[1 - \frac{1}{\sqrt{3}}\sqrt{\frac{4}{|\gamma|\left[1 - \frac{1}{2}\frac{T_D}{\theta}\right]} - 1}\right]^{1/2}, \quad (14)$$

after a sixth-order expansion of the Bessel-cardinal function. The final Eq. (14) shows that the evolution of the amplitude of

the oscillations mainly depends on the parameter γ, and we note that similar results have been found in the context of narrow-band OEOs [5–7]. The amplitude of oscillations given by Eq. (14) remains approximately valid until the breathers emerge in our system.

In order to validate our theoretical development, we compare our results on the amplitude of the oscillations with numerical simulations of Eq. (2). Bifurcation diagrams from both the theoretical and numerical analyses are presented in Fig. 2. We clearly observe in this figure that the first bifurcation occurs at $|\gamma_0|$, in the typical form of a supercritical Hopf bifurcation. The size of the limit-cycle grows continuously from zero, and increases proportionally to $\sqrt{|\gamma| - |\gamma_0|}$ for $|\gamma|$ close to $|\gamma_0| \simeq 1.031$.

4. EXPERIMENTAL OBSERVATION OF THE SLOW-SCALE LIMIT-CYCLES

The setup described in Section 2 was used to record and analyze a few of the oscillating waveforms observed under different bifurcation parameter values close to the Hopf threshold along the positive slope.

The 1550 nm Telecom DFB semiconductor laser has an output power level which can be varied from 0 to around 10 mW, thus providing a convenient way to adjust the experimental parameter β, and thus γ.

The light coming from the MZM propagates through an optical fiber and is detected by a InGaAs photodiode with a sensitivity of $S = 0.95$ A/W, at the wavelength of 1550 nm, and a bandwidth of 100 MHz. The parameter ϕ is tuned by varying V_{DC} over a $2V_{\pi DC}$ interval. The normalized feedback gain β can be tuned by varying the pump laser current from 10 to 80 mA. Figure 3 presents the experimental and numerical temporal signals in the regions (1) and (2) of Fig. 2. For values of the control parameter $|\gamma|$ just above the Hopf bifurcation, the oscillations have a shape close to the one of a sinusoidal wave. Experimentally, we observe in Fig. 4 that this sinusoidal shape is deformed when the power of the laser and therefore the gain $|\gamma|$ is increased. Such a behavior is analogous to the evolution of the oscillations in the well-known Van der Pol oscillator, where quasi-sinusoidal oscillations rapidly morph into relaxation oscillations when the gain is increased. The very good agreement between the experimental results and the numerical simulations validates the theoretical analysis
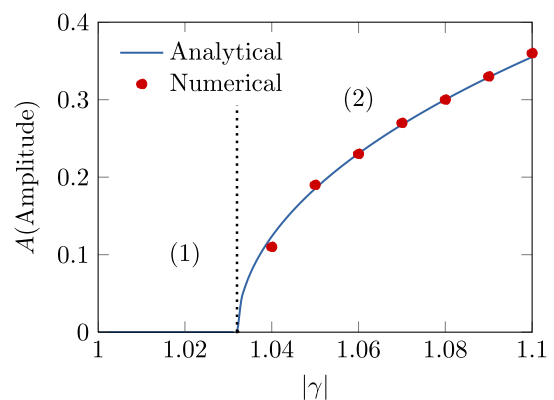
Fig. 2. Bifurcation diagram of Eq. (2) for $\phi = -\pi/4$ and $T_D = 0$. The solid line is obtained analytically from Eq. (14), while the dotted line is obtained from the numerical simulation of Eq. (2). The labels (1) and (2) indicate the two dynamical regimes.
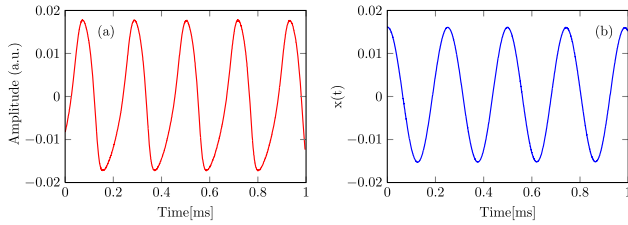
Fig. 3. Quasi-sinusoidal temporal evolution of the OEO after the Hopf bifurcation depicted in Fig. 2 ($T = 10$ µs). (a) Experimental result (pump power set just above the threshold at $P_{\text{th}} \simeq 1.2$ mW). (b) Numerical simulation of Eq. (2) for $\beta = 1.032$. Note that close to the bifurcation, the experimental and numerical plots [parts (a) and (b), respectively], display a period comparable to the theoretical value provided by Eq. (4), that is $T_0 = 2\pi/\Omega_0 = 2\pi\sqrt{\theta T_D} \simeq 250$ µs.

developed in Section 3. Note that away from the Hopf bifurcation, the numerical experimental transitions are sharper than the numerical ones because the filters used experimentally have a sharper profile (steeper edges) than the low-order bandpass filters considered in the model.

We will now focus on the evolution of the period of the oscillations when the control parameter is changed. In the presence of delay, the complexity of the dynamics does not allow for a simple mathematical analysis. We will therefore start by studying the case where the delay can be neglected ($T_D = 0$). In Section 6, we will show that the case $T_D = 0$ enables an in-depth understanding of the general case where T_D is not null.

5. EVOLUTION OF THE PERIOD WITH γ IN THE CASE $T_D = 0$

In this section, we study the dependence of the period with the parameters β and ϕ. In the first case, β is varied while ϕ is fixed to $-\pi/4$ (symmetric wave oscillations). In the second case, we maintain the parameter β fixed but we vary ϕ, and here, strongly asymmetric oscillations emerge. In both cases, we compare analytical results with the numerical ones.

A. Evolution of the Period with β
We first rewrite Eq. (2) under the form

$$\dot{y} = x, \tau\dot{x} = -x - \frac{1}{\theta}y + \beta\{\cos^2[x + \phi] - \cos^2(\phi)\}. \tag{15}$$

Note that in the above equation, the term $-\beta\cos^2(\phi)$ has been added on the right-hand side of the equation ruling the dynamics of x. This term, which has in fact no impact on the long-term dynamics of the system (it is a constant term, which is progressively eliminated by the bandpass filtering of the
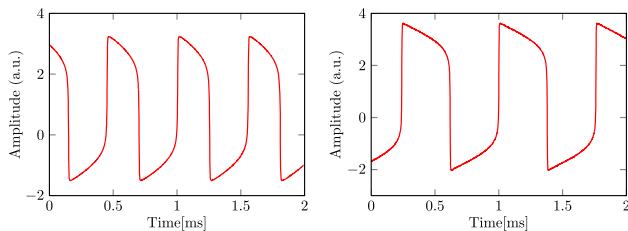

Fig. 4. Typical experimental timetraces of the relaxation-like slow-scale dynamics of the OEO far away from the Hopf bifurcation. The period T_{exp} is found to vary significantly with the gain, still having the same order of magnitude as the theoretical Hopf period T_0. (Left) $T_{\text{exp}} \simeq 560$ µs. (Right) $T_{\text{exp}} \simeq 760$ µs.

system), is nevertheless physically convenient because it enables one to immediately spot that $x = 0$ is a fixed point in the system.

In this equation, we have two time scales (slow and fast). The slow manifold is obtained in the limit $\tau \to 0$ in Eq. (15), yielding

$$z = -x + \beta\{\cos^2[x + \phi] - \cos^2(\phi)\}, \tag{16}$$

where $z = (1/\theta)y$, and from Eqs. (15) and (16), we can derive

$$\dot{x} = -\frac{1}{\theta}\frac{x}{1 + \beta\sin(2x + 2\phi)}. \tag{17}$$

In the phase space, slow transition dynamics end when the velocity tends to infinity, and this corresponds to

$$1 + \beta\sin(2x + 2\phi) = 0. \tag{18}$$

The above equation gives the two critical points in Fig. 5, namely, x_N and x_Q following:

$$x_N = -x_Q = \frac{1}{2}\arccos\left(\frac{1}{|\gamma|}\right). \tag{19}$$

The maximum and the minimum values of the amplitude of the wave oscillation in Fig. 5 are deduced from Eq. (14)

$$x_M = -x_P = \sqrt{3}\left[1 - \frac{1}{\sqrt{3}}\sqrt{\frac{4}{|\gamma|} - 1}\right]^{1/2}. \tag{20}$$

We can now compute the period of the system as the sum of the durations of the two slow dynamical phases of the oscillation beginning at M and ending at Q:

$$T_{\text{Sym}} = T_{M \to N} + T_{P \to Q}, \tag{21}$$

where $T_{M \to N}$ and $T_{P \to Q}$ represent the durations of the two slow transitions. The duration of the fast time transition is considered negligible, thereby yielding $T_{N \to P} \simeq 0$. For the evaluation of the duration of the slow time scale phase, we use Eq. (14) to obtain
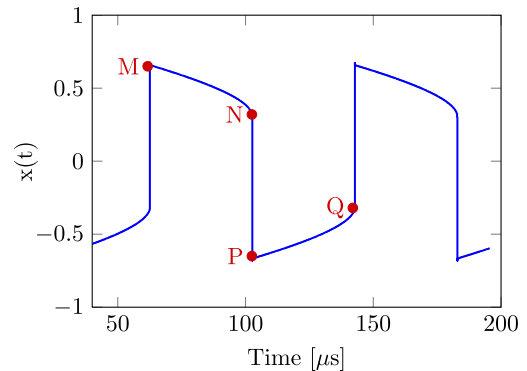

Fig. 5. Typical time evolution of x in Eq. (15) for $\beta > 1$, $\phi = -\pi/4$, and $T_D = 0$. Note the symmetric nature of this numerical timetrace.

$$T_{M \to N} = -\theta \int_{x_M}^{x_N} \frac{1 + \gamma \cos(2x)}{x} \, dx. \tag{22}$$

Due to the symmetric nature of the oscillations we always have $T_{M \to N} = T_{P \to Q}$, and the integration of Eq. (22) gives

$$T_{\text{Sym}}(\gamma) = 2\theta \left[\ln\left(\frac{x_M}{x_N}\right) + \gamma [\text{Ci}(2x_M) - \text{Ci}(2x_N)] \right], \tag{23}$$

where Ci is the cosine-integral function. It is possible to integrate numerically Eq. (23) when the endpoints of the integral are given or well known. In Fig. 5, we show the time evolution of Eq. (15) when the value of β is higher than 1. This oscillation presents a symmetric wave shape, with equal absolute values for the extremal amplitudes. In Fig. 6, we have displayed the evolution of the period of this symmetric wave oscillation, which is obtained using the numerical simulation of Eq. (15) and the analytical expression of Eq. (23). We observe an excellent agreement between the numerical and analytical results. It is also important to note that in this case of null time-delay, the evolution of the period is almost perfectly a linear function of β.

B. Evolution of the Period with ϕ

In this subsection, we study the evolution of the period of the system when the bias voltage $V_{\pi \text{DC}}$ is tuned, and this is equivalent to change the value of the parameter ϕ. In the general case, the variation of ϕ influences the shape of the wave. This was theoretically and experimentally analyzed in [15], where strongly asymmetric square waves with a period close to one delay are observed in the OEO. The solution we focus on in this article (slow motion instead of a one-delay period) also exhibits asymmetry with respect to parameter ϕ. Let us consider the period of the asymmetric wave oscillation to be T_{Asym}. This period can be approximated by the sum of the two slow-scale phases occurring in Fig. 7 during the transition from A to B ($T_{A \to B}$), and from C to D ($T_{C \to D}$), according to

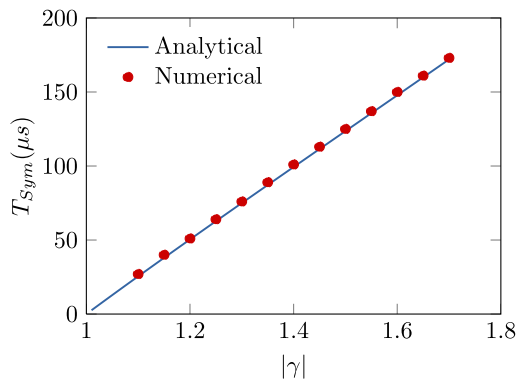$$T_{\text{Asym}} = T_{A \to B} + T_{C \to D} \tag{24}$$

with

Fig. 6.   Evolution of the period of the symmetric wave oscillation for $T_D = 0$ and $\phi = -\pi/4$. The solid line is obtained with the analytical simulation of Eq. (23), while the dots stand for the numerical simulations of Eq. (15).

$$T_{A \to B} = \int_{x_A}^{x_B} f(x) \, dx,$$

$$T_{C \to D} = \int_{x_C}^{x_D} f(x) \, dx, \tag{25}$$

where

$$f(x) = -\theta \frac{1 + \beta \sin(2x + 2\phi)}{x}. \tag{26}$$

Note that asymmetry implies $T_{A \to B} \neq T_{C \to D}$. The integrals in Eq. (25) give the following expression of the period of the system:

$$\begin{aligned} T_{\text{Asym}}(\phi) = &-\theta \ln\left(\frac{x_B x_D}{x_A x_C}\right) \\ &- \theta\beta \sin 2\phi [\text{Ci}(2x_B) + \text{Ci}(2x_D) \\ &- \text{Ci}(2x_A) - \text{Ci}(2x_C)] \\ &+ \theta\beta \cos 2\phi [\text{Si}(2x_B) + \text{Si}(2x_D) \\ &- \text{Si}(2x_A) - \text{Si}(2x_C)], \end{aligned} \tag{27}$$

where Si is the sine-integral function. In the above equation, the integral domain boundaries x_A, x_B, x_C, and x_D are unknown at this stage. In order to compute Eq. (27), these four quantities have to be determined. Using the same reasoning as in the preceding subsection, the equation $1 + \beta \sin(2x + 2\phi) = 0$ is solved in order to determine x_B and x_D. It results that

$$x_B = -\frac{1}{2} \arcsin\left(\frac{1}{\beta}\right) - \phi,$$

$$x_D = \frac{1}{2}\left[-\pi + \arcsin\left(\frac{1}{\beta}\right)\right] - \phi. \tag{28}$$

The values of x_B and x_D shown in Fig. 7 are, respectively, positive and negative. Let us now determine the maximum and the minimum values x_A and x_C of the wave of Fig. 7. We first evaluated $z(x_B)$ and $z(x_D)$ from Eq. (16) using the values of x_B and x_D computed in Eq. (28). The analysis of Fig. 8 shows that $z(x_B) = z(x_C)$ and $z(x_D) = z(x_A)$, and these equalities can be exploited to yield

$$-x_A + \beta[\cos^2(x_A + \phi) - \cos^2(\phi)] = z(x_D),$$

$$-x_C + \beta[\cos^2(x_C + \phi) - \cos^2(\phi)] = z(x_B). \tag{29}$$
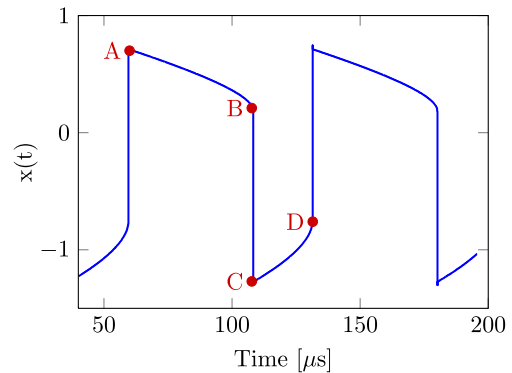
Fig. 7.   Temporal evolution of Eq. (15) for $\phi = -0.51$ and $T_D = 0$. Note the asymmetric nature of this numerical timetrace.
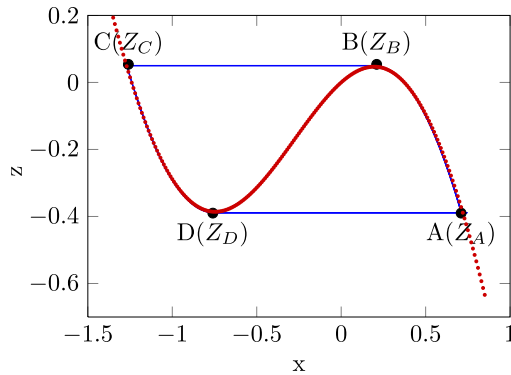
Fig. 8.   Plot of the x–z phase space, for $\phi = -0.51$ and $T_D = 0$. The blue continuous line is the numerical simulation of Eq. ([15](#)), and the red-dotted line is the numerical simulation of Eq. ([16](#)).

The resolution of Eq. ([29](#)) allows us to determine $x_A > 0$ and $x_C < 0$. However, it is not possible to have the simple expression of these extrema. Numerical simulation is required to determine their numerical values. The computation of Eqs. ([27](#)), ([28](#)), and ([29](#)) when β is fixed and ϕ is varied is represented in Fig. [9](#).

It results from this figure that the analytical expression of Eq. ([27](#)) coincides with the numerical simulation of the Eq. ([15](#)), and we observe that the evolution of the period with ϕ is a parabolic shape. We also see in Fig. [9](#) that the minimum value of the period for a fixed value of β corresponds to the symmetric oscillations with $\phi = -\pi/4$.

6. DISCUSSION OF THE CASE OF THE OEO WITH DELAY ($T_D \neq 0$)

We here discuss the evolution of the period of the system when the delay is considered. In order to compute this, we have to take into account the fast time scale dynamics which are not negligible anymore. The resulting period is $T_{\text{sys}} = 2T_{\text{slow}} + 2T_{\text{fast}}$, and both contributions have to be analyzed in detail. A multiple time scale approach can be used for this purpose [11].

Slow manifolds are (locally) invariant subsets along which the speed is commensurate with the slow time scale in slow–fast systems. In many systems, trajectories spend most of their time attracting slow manifolds—making rapid transitions from one slow manifold to another [21–23]. Let us consider
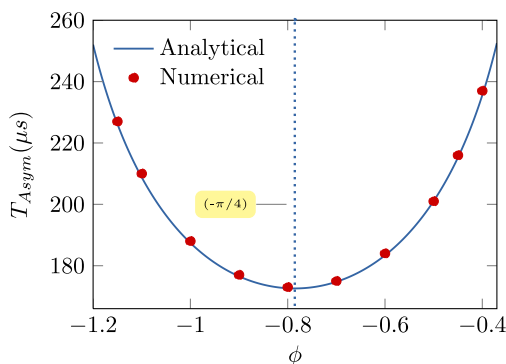

Fig. 9.   Evolution of the period of the asymmetric wave oscillation and $T_D = 0$. The solid line is obtained by the analytical simulation of Eq. ([28](#)), while the dots stand for the numerical simulation of Eq. ([15](#)).

that the slow time is $t_1 = \epsilon_0 t$. The differentiation of Eq. ([2](#)) with respect to t_1 yields

$$\frac{dx(t_1)}{dt_1} - \beta \, \cos(2x(t_1 - \epsilon_0 T)) \frac{dx(t_1 - \epsilon_0 T_D)}{dt_1}$$
$$+ \frac{x(t_1)}{\theta \epsilon_0} = 0, \tag{30}$$

where the terms in $O(\epsilon_0^3)$ have been neglected and $\phi = -\pi/4$. The time delay variable contained in Eq. ([30](#)), can be simply approximated as

$$x(t_1 - \epsilon_0 T_D) \approx x(t_1) + \eta(\epsilon_0, T_D, x_{\max}), \tag{31}$$

where η is a very small function (with respect to x) having the following properties: (i) $\eta \neq 0$ when $T_D \neq 0$ and (ii) $\eta = 0$ when $T_D = 0$. The variable $x(t_1)$ can be deduced from the study done above, but the principal difficulty is to determine the function η as a function of the delay. Unfortunately, there is no mathematical theory able to analytically determine this functional dependence.

For the analysis of the fast manifold transition, it is rather convenient to take the fast time $t_2 = t/\epsilon_0$. The differentiation of Eq. ([30](#)) with respect to t_2 yields

$$\frac{d^2x(t_2)}{dt_2^2} + \frac{dx(t_2)}{dt_2} - \beta \, \cos[2x(t_2 - T_D/\epsilon_0)]$$
$$\times \frac{dx(t_2 - T_D/\epsilon_0)}{dt_2} = 0, \tag{32}$$

and Eq. ([32](#)) can enable us to track the fast manifold behavior of the oscillation.

7. CONCLUSION

In this article, we have investigated the slow-scale dynamics of a wideband optoelectronic oscillator and analyzed the evolution of the amplitude and period of the Hopf-induced limit-cycle with respect to the gain and the offset phase. It has been evidenced that the dynamical features of the slow-scale limit-cycle are indeed significantly modified by these parameters. We have successfully compared some of our theoretical results with numerical simulations and experimental measurements. We have shown that in the case of null time-delay, the evolution of the period is a linear function of the gain and parabolic with respect to the offset phase. Our investigations have also outlined the link between the two-dimensional dynamics of the zero-delay system and the infinite-dimensional dynamics of the delayed system.

Future work will focus on a full characterization of the route to chaos in these systems where the three main time scales are distributed in a logarithmic-like fashion, as well as on the multiscale nonlinear dynamics of other OEO architectures [24–26].

REFERENCES

1. T. Erneux, *Applied Delay Differential Equations* (Springer, 2010).
2. M. Lakshamanan and D. V. Senthikumar, *Dynamics of Nonlinear Time-Delay Systems* (Springer, 2011).
3. L. Larger, "Complexity in electro-optic delay dynamics: modelling, design and applications," Phil. Trans. R. Soc. A **371**, 20120464 (2013).
4. M. C. Soriano, J. Garcia-Ojalvo, C. R. Mirasso, and I. Fischer, "Complex photonics: dynamics and applications of delay-coupled semiconductors lasers," Rev. Mod. Phys. **85**, 421–470 (2013).
5. X. S. Yao and L. Maleki, "Optoelectronic microwave oscillator," J. Opt. Soc. Am. B **13**, 1725–1735 (1996).
6. Y. K. Chembo, L. Larger, H. Tavernier, R. Bendoula, E. Rubiola, and P. Colet, "Dynamic instabilities of microwaves generated with optoelectronic oscillators," Opt. Lett. **32**, 2571–2573 (2007).
7. Y. K. Chembo, L. Larger, and P. Colet, "Nonlinear dynamics and spectral stability of optoelectronic oscillators," IEEE J. Quantum Electron. **44**, 858–866 (2008).
8. J.-P. Goedgebuer, P. Levy, L. Larger, C.-C. Chen, and W. T. Rhodes, "Optical communication with synchronized hyperchaos generated electrooptically," IEEE J. Quantum Electron. **38**, 1178–1183 (2002).
9. A. Argyris, D. Syvridis, L. Larger, V. Annovazzi-Lodi, P. Colet, I. Fischer, J. Garcia-Ojalvo, C. R. Mirasso, L. Pesquera, and K. A. Shore, "Chaos-based communications at high bit rates using commercial fibre-optic links," Nature **438**, 343–346 (2005).
10. Y. C. Kouomou, P. Colet, L. Larger, and N. Gastaud, "Chaotic breathers in delayed electro-optical systems," Phys. Rev. Lett. **95**, 203903 (2005).
11. Y. K. Chembo, L. Larger, R. Bendoula, and P. Colet, "Effects of gain and bandwidth on the multimode behavior of optoelectronic microwave oscillators," Opt. Express **16**, 9067–9072 (2008).
12. A. B. Cohen, B. Ravoori, T. E. Murphy, and R. Roy, "Using synchronization for prediction of high-dimensional chaotic dynamics," Phys. Rev. Lett. **101**, 154102 (2008).
13. K. E. Callan, L. Illing, Z. Gao, D. J. Gauthier, and E. Scholl, "Broadband chaos generated by an optoelectronic oscillator," Phys. Rev. Lett. **104**, 113901 (2010).
14. B. Ravoori, A. B. Cohen, J. Sun, A. E. Motter, T. E. Murphy, and R. Roy, "Robustness of optimal synchronization in real networks," Phys. Rev. Lett. **107**, 034102 (2011).
15. L. Weicker, T. Erneux, O. D'Huys, J. Danckaert, M. Jacquot, Y. Chembo, and L. Larger, "Strongly asymmetric square waves in a time-delayed system," Phys. Rev. E **86**, 055201(R) (2012).
16. R. Martinenghi, S. Rybalko, M. Jacquot, Y. K. Chembo, and L. Larger, "Photonic nonlinear transient computing with multiple-delay wavelength dynamics," Phys. Rev. Lett. **108**, 244101 (2012).
17. L. Weicker, T. Erneux, O. D'Huys, J. Danckaert, M. Jacquot, Y. K. Chembo, and L. Larger, "Slow–fast dynamics of a time-delayed electro-optic oscillator," Phil. Trans. R. Soc. A **371**, 20120459 (2013).
18. K. Ikeda, "Multiple-valued stationary state and its instability of the transmitted light by a ring cavity system," Opt. Commun. **30**, 257–261 (1979).
19. K. Ikeda, H. Daido, and O. Akimoto, "Optical turbulence: chaotic behavior of transmitted light from a ring cavity," Phys. Rev. Lett. **45**, 709–712 (1980).
20. K. Ikeda and M. Matsumoto, "Study of a high-dimensional chaotic attractor," J. Stat. Phys. **44**, 955–983 (1986).
21. Z. H. Wang, "An iteration method for calculating the periodic solution of time-delay systems after a Hopf bifurcation," Nonlinear Dyn. **53**, 1–11 (2008).
22. J. Guckenheimer and P. Holmes, *Nonlinear Oscillations, Dynamical Systems and Bifurcation of Vector Fields* (Springer-Verlag, 1983).
23. Z. H. Wang and H. Y. Hu, "Pseudo-oscillator analysis of scalar nonlinear time-delay systems near a Hopf bifurcation," Int. J. Bifurcation Chaos Appl. Sci. Eng. **17**, 2805–2814 (2007).
24. Y. K. Chembo, A. Hmima, P.-A. Lacourt, L. Larger, and J. M. Dudley, "Generation of ultralow jitter optical pulses using optoelectronic oscillators with time-lens soliton-assisted compression," J. Lightwave Technol. **27**, 5160–5167 (2009).
25. R. M. Nguimdo, Y. K. Chembo, P. Colet, and L. Larger, "On the phase noise performance of nonlinear double-loop optoelectronic microwave oscillators," IEEE J. Quantum Electron. **48**, 1415–1423 (2012).
26. A. Coillet, R. Henriet, P. Salzenstein, K. P. Huy, L. Larger, and Y. K. Chembo, "Time-domain dynamics and stability analysis of optoelectronic oscillators based on whispering-gallery mode resonators," IEEE J. Sel. Top. Quantum Electron. **19**, 6000112 (2013).